 International Journal of Turbo and Jet Engines, 13, 277–293 (1996)

Vortical Structures in Channel Flows with a Backward-Facing Step

Tony W.H. Sheu*, T.P. Chiang and S.F. Tsai
Department of Naval Architecture and Ocean Engineering, National Taiwan University, 73 Chou-Shan Road, Taipei, Taiwan, R.O.C.

Abstract

The aim of this study was to conduct a detailed numerical analysis of steady-state Navier-Stokes equations to broaden our knowledge of the vortical flow structure in the channel. The problem considered is that of the laminar flow of an incompressible fluid through a straight channel with a backward-facing step. This step is configured as having an expansion ratio of $\gamma = 1.9423$ in channels with different channel widths of B. Finite volume solutions for this backward-facing step problem were obtained on the basis of different span ratios, $B/h = 2$, 4, 6, 10, and Reynolds numbers, $Re = 100$, 389, and 800. In this study, we elaborate on the case of $Re = 389$ due to lack of space. Inspired by the success of Lighthill who proposed a method with a rigorous mathematical foundation for studying kinematically possible flows, we apply the topology theory to analyze the computed three-dimensional vector field. The inferred 'oil-flow' streamlines improve visualization of the flow field and help sketch the complicated flow patterns by clarifying the three-dimensional flow separation just behind the step, the formation of secondary eddies in the transverse plane, and recirculating bubbles attached to the roof of the channel. Notably addressed is the separation-reattachment phenomenon that emanates only from the roof near the two end walls.

Nomenclature

u_i	velocity component along the i-direction
p	pressure
x_m	coordinate along the m-direction
Re	Reynolds number
t	time
ν	kinematic viscosity
u_{mean}	inlet mean velocity
h	height of the upstream channel
H	height of the downstream channel
B	width of the channel
γ	expansion rating ($= H/h$)
S	non-dimensional step height ($= \gamma - 1$)
x_1	reattachment length, as measured from the step, of the primary eddy
x_4	separation length, as measured from the step, of the roof eddy
x_5	reattachment length, as measured from the step, of the roof eddy
N_x	number of grid points in the streamwise direction

1. Introduction

In many situations in nature as well as in science and industry, fluid flows characterized as having separation are encountered. Examples include flows around buildings, microelectronic circuit boards, conjugated heat exchangers, and those in ducts for industrial use. A better understanding of the mechanism leading to flow reversal would yield better understanding of the impact of the separation-reattachment flow structure on the evolving flow passage. To achieve this goal, problems of this class which accommodate simple geometry are most suitable for study.

Channel flows with a backward-facing step have been the focus of intensive study over the last few decades and have been the subject of an international workshop /1/. Specific to this flow is that it is one of a few simple examples which accommodate rather complex flow physics in a channel having a simple configuration. There are two reasons why this problem has received considerable attention. Firstly, this flow is rich in physics and is, thus, physically as well as practically

* Author to whom correspondence should be addressed. Fax number: 886-2-3929885

important. Within the channel, there exists a shear layer separated from the step edge, a recirculating flow region just behind the step, followed by a region with a recirculating separation-reattachment flow attached to the roof of the channel, and gradual development of the channel flow further downstream. Gaining an understanding of this expansion flow is, thus, of importance to better understand shear stresses and heat transfer rates which serve as controlling factors in designing many industrial flow devices. We will also consider this problem computationally important since this problem is regarded as a prototype for assessment of numerical models on incompressible viscous flows.

Physical importance has stimulated a number of experimental calibrations /2-9/, among which the experimental data obtained by Armaly *et al.* /3/ are most frequently referenced. This wealth of experimental data has permitted a very detailed comparison to be performed. In the past, the focus was on the two-dimensional context /1,10/, and comparatively few studies focused on three-dimensional simulations /2,11-18/. It is this scarcity of three-dimensional numerical studies which motivated us to conduct this study. While previous efforts have shed light on some fundamental features of the backward-facing step flow, questions still remain unanswered, such as the broad pattern of the recirculating flow structure behind the step. The present work was directed towards revealing the detailed three-dimensional flow structure evolving in the flow passage. To achieve this goal, we adopted a topological theory in studying the computed three-dimensional vector field.

The remaining sections of this paper are organized as follows. Section 2 gives a brief description of the working equations, problem specifications, and the segregated type algorithm which is used to solve the finite volume discretization equations iteratively. To present a clear picture of the vortical flow structure, we exploit the theory of topology, as given in Section 3, to study the limiting streamlines or skin-friction lines. The justification for using this analysis code is presented first in Section 4.1 in order to give readers a better idea of the solution quality this code can offer. Numerical results and conclusions are presented in Section 4, which provides insight into the evolution of vortical flows as the Reynolds number and width of the channel vary. In Section 5, we present a conclusion.

2. Theoretical Formulation

In the absence of a body force, a Newtonian fluid characterized as having constant kinematic viscosity ν was chosen as the working media. The governing equations were Navier-Stokes equations which are constrained by flow incompressibility. This demands the use of a continuity equation. For this study, numerical modelling was performed under conditions pertaining to the steady and laminar assumptions. The following working equations are thus the consequence:

$$\frac{\partial}{\partial x_m}(u_m u_i) = \frac{\partial p}{\partial x_i} + \frac{1}{Re}\frac{\partial^2 u_i}{\partial x_m \partial x_m}, \qquad (1)$$

$$\frac{\partial u_i}{\partial x_i} = 0 . \qquad (2)$$

A plausible reason for choosing the velocity-pressure formulation is that this setting can offer well-posed closure boundary conditions /19/. In the above dimensionless primitive-variable equations, we denote working variables u_i, as the velocity components ($i = 1 \sim 3$), and p as the isotropic pressure. In what follows, the Reynolds number is defined to be $Re = u_{mean} \cdot 2h/\nu$, where h denotes the height of the upstream channel. In equations (1-2), lengths are normalized with h while velocities are normalized by the inlet mean velocity, u_{mean}, which is the result of an entry flow in a straight rectangular channel with a cross-sectional area of $h \times B$.

We of necessity transform working equations into their algebraic counterparts so that they are amenable to computer simulation. To alleviate the well-known even-odd pressure oscillations for the incompressible fluid flow, we advocate the use of staggered grids. According to the findings of Harlow and Welch /20/, the grid used offsets the velocities with half a mesh size in their respective coordinate directions from the pressure. While staggered mesh adds considerably to the pro-

gramming, this grid setting is widely used for incompressible analyses because enforcement of the compatibility condition which is required to suppress pressure oscillations is avoided.

Use of primitive variables to simulate incompressible Navier-Stokes equations may considerably complicate the analysis because of the absence of pressure unknowns in the continuity equation. Not only will this absence tend to increase the condition number for the discrete system, but it will also yield more zero diagonals, thus causing the diagonal dominance to deteriorate. This presents a challenging task of solving algebraic equations in a strongly completed manner. As a compensation for the mixed formulation, segregated solution algorithms have been exploited by many researchers. The algorithmic idea of this class of approaches is to enforce satisfaction of the divergence-free constraint condition through pressure correction, which is cast in the form of a Poisson equation. By doing so, the continuity equation is asymptotically ensured. This equation provides a mechanism for incorporating the incompressibility constraint into the formulation through multiply-stage equations. In general, use of this pressure correction algorithm can considerably reduce the storage demand for the matrix equations encountered. Without loss of stability, the semi-implicit scheme of SIMPLE /21/, as applied in the present study, provides the same steady-state solution with less computational cost compared to the equivalent explicit scheme.

False diffusion errors are well known as another class of numerical difficulties for the solutions of (1-2). Under conditions where grid lines are increasingly skewed with respect to streamlines, the quality of the computed solution deteriorates due to the introduction of false diffusion errors, grossly polluting the flow physics over the entire domain. Deterioration in accuracy is particularly severe under high Reynolds number circumstances. To remedy this defect, we apply here the upwind scheme of Leonard /22/ to model nonlinear terms defined in a domain which is non-uniformly discretized. As was the case with the elliptic problem, both diffusive fluxes and pressure gradients are approximated by a second-order centered scheme. Also, discretization errors arising from curvilinear coordinate transformation are generally considerable and hard to resolve for configurations involving an abrupt change or for curvilinear lines having a marked change of curvature. As a consequence, we conduct analysis here in a Cartesian coordinate system in the hope of obtaining the detailed flow physics.

3. Topological Study on Three-Dimensional Vector Field

With the ever-increasing speed of computers and cost effective computations, three-dimensional calculations have become feasible. This adds renewed interest to visualization of flow complexities because three-dimensional data are considerable, and it is difficult to visualize vector fields using conventional methods. This difficulty has prompted numerous researchers to develop new methodologies in the hope of easily providing a description of the pertinent flow structure from the computed solutions. There are several methods to choose from. Among them, the use of graphical representations of the flow field underlying the helicity /23/ and the topology theory of continuous vector fields /24,25/ have been shown to achieve this goal and have gained wide acceptance. For a historical survey of this subject, see Yates and Chapman /26/ for greater detail.

Guided by the findings of Poincare /27/, we explored the kinematics of a fluid flow. The idea of relating the differential equations to the topology of vector fields is to expand a given vector, $\underline{\mathbf{f}}$, with respect to a specific point $\underline{\mathbf{x}}^0$, known as the singular point. By definition, singular points are those which accommodate the property of $f_i\big|_{\underline{\mathbf{x}}=\underline{\mathbf{x}}^0} = 0$. Bearing this definition in mind, the Taylor series expansion of $\underline{\mathbf{f}}$ about $\underline{\mathbf{x}}^0$ is as follows:

$$f_i = (x_j - x_j^0)\frac{\partial f_i}{\partial x_j} + h.o.t. \qquad (3)$$

Provided that the vector field $\underline{\mathbf{f}}$ is sufficiently smooth to allow a continuous differentiation, eigenvalues and the associated eigenvectors of the matrix $\frac{\partial \underline{\mathbf{f}}}{\partial \underline{\mathbf{x}}}$ determine the behavior of $\underline{\mathbf{f}}$ around the

singular point $\underset{\sim}{x}^0$. A brief introduction to classification of singular points will be given later in this section.

Lighthill /25/ was among the first researchers to apply the qualitative theory of differential equations in the field of fluid dynamics. He chose skin-friction lines as the targeted vector field. Parallel to the work of Lighthill, Legendre /24/ took streamlines into consideration in his topological study. These two classes of topological studies have been frequently used to explore flow dynamics because of the existence of the mathematically rigorous foundation. The flow topology rendered from skin-friction lines corresponds to the experimental oil streak on the surface. In view of the fact that limiting streamlines are equivalent to skin-friction lines, we can conduct topological study through the use of limiting streamlines. As pointed out earlier, three-dimensional flows can also be sketched by conducting graphical visualization of the scalar quantity. The density of the helicity or the normalized helicity is frequently used in this regard /23/. Due to space considerations, we will concentrate in this paper only on topological study of skin-friction lines for the surface topology and on streamlines in regions sufficiently distant from the surfaces.

We will examine the flow topology in two areas. In the surface topology context, singular points can be classified as saddles and nodes. Saddle points are defined as singular points which have two real eigenvalues of different signs. The skin-friction line field approaches the saddle point along the negative eigendirection while it recedes along the positive eigendirection. Nodal points can be further divided into two groups. Nodes (or regular nodal points) are those with real eigenvalues having the same sign. Attracting nodes are associated with the negative real eigenvalue. As to repelling nodes, the situation is reversed. Foci are also labeled as singular points, whose eigenvalues are, on the other hand, conjugate complex. Depending on the sign of the real part of the eigenvalue, flows spiral either in or out of the singular point.

In three dimensions, streamlines approach (recede from) a three-dimensional saddle along a plane spanned by two eigenfunctions having the same sign, and recede (approach) from a line having the same direction as the third eigenfunction /28/. Similar to two-dimensional classification of critical points, three-dimensional nodes are those defined as having three reals while irregular nodes (or spiral saddles) accommodate a pair of conjugate complex eigenvalues and a real eigenvalue. We can follow the same rule to classify critical points either to repel or attract nodes and spirals. The topological results presented in the result section are rooted in some fundamentals discussed in this section.

4. Computed Results

4.1. Validation of analysis code

In attempting to accurately explore the flow physics, the first step is to validate the analysis code employed. In this regard, we consider here the geometrically simple problem /29/. In a cubic Ω ($-1 \leq x,y,z < 1$), boundary values are specified according to the following divergence-free velocities:

$$u = -a[e^{a\,x}\sin(a\,y \pm d\,z) + e^{a\,z}\sin(a\,x \pm d\,y)],$$

$$v = -a[e^{a\,y}\sin(a\,z \pm d\,x) + e^{a\,x}\sin(a\,y \pm d\,z)], \quad (4)$$

$$w = -a[e^{a\,z}\sin(a\,x \pm d\,y) + e^{a\,y}\sin(a\,z \pm d\,x)].$$

In this study, we consider $a = \frac{d}{2} = \frac{\pi}{4}$ and $Re = 1000$. The employed QUICK-type upwind discretization scheme and semi-implicit solution algorithm are assessed by examining nodal errors which are cast in an L_2-norm form. With continuous refinement of grid spacings, we can compute the rate of convergence. According to the errors computed against the grid spacings, namely h = 1, 1/3, 1/9, 1/27, the rate of convergence can be derived and is clearly seen in Fig. 1. Through this test, taking finite volume solutions computed on the basis of h = 1/27 as exact, the validity of the analysis code is confirmed. This provides us with sufficient confidence to proceed with the analysis of the three-dimensional expansion flow over a step.

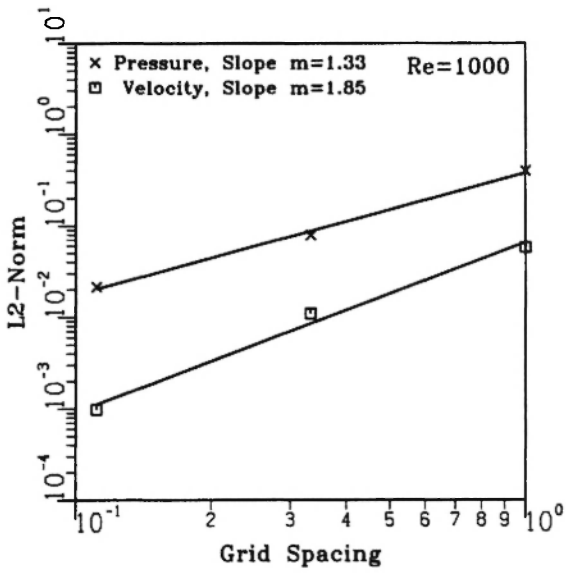

Fig. 1: Grid convergence test for the steady Navier-Stokes equations presented in Section 4.1.

4.2. Three-dimensional backward-facing step problem

The problem we will deal with is the flow expansion in a water-filled rectangular channel. The channel under investigation is configured as having a backward-facing step with height S = 0.9423, as shown in Fig. 2. Upstream of this step, there is a straight channel with a height of h = 1 and a channel with a larger height H = 1.9432 downstream of the step. In our three-dimensional analysis, we prescribe at the inlet a discrete fully developed velocity profile. Experimental study has revealed that the downstream flow evolution is insensitive to this parabolic assumption of the inlet flow specification for cases where the Reynolds number becomes larger than 200 /2/. No-slip boundary conditions for velocities u_i are specified at the two end walls, roof and floor of the channel. As is usual in dealing with inflow-outflow internal flow problems, we impose a floating outflow boundary condition at the synthetic plane. Depending on the Reynolds numbers investigated, an attempt to obtain an accurate prediction demands that synthetic

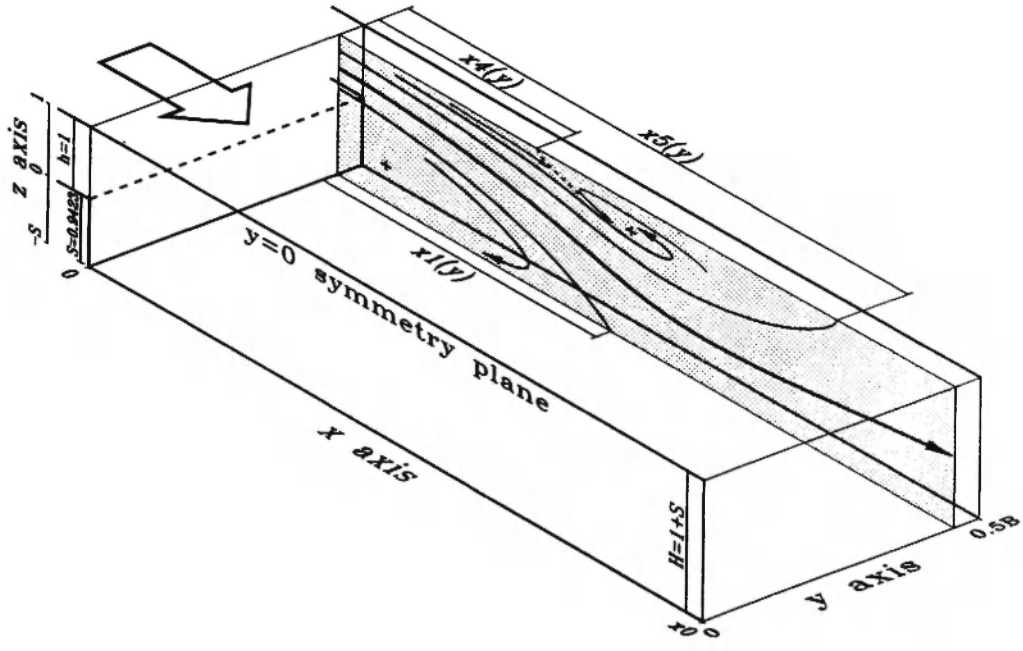

Fig. 2: Geometric definition and physical description of the flow feature.

planes be truncated at different locations that are sufficiently far away from the step.

On physical grounds, we stretch mesh points near the two end walls and the step plane to resolve high gradient velocity profiles. Within half of the channel, the domain is covered with $N_x \times 17 \times 40$ mesh points in the narrow case of $B = 2$ and $N_x \times 37 \times 40$ points in the wider case of $B = 10$. In our study, the values of N_x are, respectively, chosen as 60, 80, and 100 for the Reynolds numbers 100, 389, and 800. As experimental evidence has revealed /3/, the investigated backward-facing problem remains laminar for Reynolds numbers below 1200, so the present analysis avoids invoking turbulence modelings and, thus, simplifies the analysis.

4.2.1. Flow patterns in the channel

Figs. 3-5 plot the streamwise velocity profiles at the symmetry plane, starting from the step and continuously extending to the truncated outlet. On increasing the width of the channel, the velocity profiles progressively develop into those computed on the basis of two-dimensional analysis or calibrated by Armaly *et al.* /3/. Agreement is quite good except in regions which range roughly between x_4 and x_5. This finding suggests that the span of the channel has a marked influence on the downstream flow development. For the sake of comparison, we also summarize in Fig. 6 some two-dimensional numerical results; also included are the experimental data of Armaly *et al.* /3/ for the same step geometry with an expansion ratio of $\gamma = 1.9423$. Irrespective of the numerical approach followed, there exists consistent underestimation of the recirculation length x_1 when the value of the Reynolds number is above 600. As the Reynolds number is beyond the characteristic value, we doubt the bifurcation of the steady, two-dimensional laminar flow into a three-dimensional flow is the primary source that leads to the discrepancy between the two-dimensional numerical solutions and experimental data.

Another way to elucidate a complex three-dimensional flow structure is to trace particles. Fig. 7 shows several computed stream-ribbons released from selected locations in the channel. Viewed from the span direction, particle tracers seeded near the end wall spiral, with an increasingly larger radius, towards the symmetry plane. As the symmetry plane is approached, the spiraling particle is lifted up, followed by a nearly two-dimensional plane motion. Other seeded particles proceed downstream in a much simpler fashion.

As Fig. 8 reveals, as fluids flow over the roof eddy, which is attached only to the end wall, an end wall running velocity component is induced near the bottom wall while a symmetry plane running velocity component is induced near the roof of the channel. This suggests the formation of a secondary flow structure at the transverse plane, say at $x = 8$. It is the presence of a roof eddy which explains why the topology of the oil-pattern at the end wall is as that plotted in Fig. 8. Also important to note is that the primary eddy structure behind the step and the previously mentioned upward oil-pattern, arising from the roof eddy, constitute the possible formation of a saddle point. The presence of a secondary flow near the end wall also explains why a repelling-spiral appears. In some regions in the downstream channel, a pair of counter-rotating vortices, one stretched near the roof of the channel and the other confined to the region near the end wall, are clearly seen at the streamwise plane $x = 10$. This is followed by larger extension of vortices but with decreasing intensity. We also plot streamlines in Fig. 9 to show that the presence of counter-rotating vortices is closely related to the separation-reattachment bubble at the roof of the channel. In contrast with two-dimensional areas, these lines are not closed due to the presence of a spanwise velocity component. As shown in Fig. 10, which plots the pressure distribution on the channel walls, this is strongly indicative of the presence of flow reversals in the channel.

4.2.2. Exploration of flow structure – a topological study

To give a global picture of the expansion flow over a step, we begin by plotting limiting streamlines, at planes $z = 0.9999$, $z = -0.9423$, $y = 4.9999$, and $x = 10^{-4}$, for the case of $Re = 389$. As Fig. 11 indicates, in the channel with $B = 10$, a singular

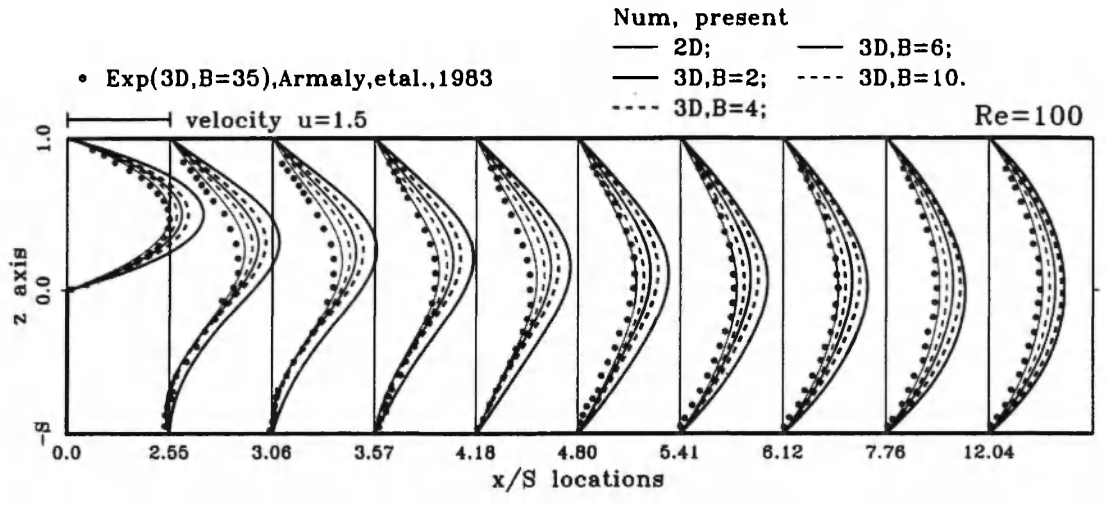

Fig. 3: Comparison study of streamwise-velocity profiles with those of Armaly *et al.* at the symmetry plane for the case conditions of Re = 100 and B = 2, 4, 6, 10, and ∞ (or 2D analysis).

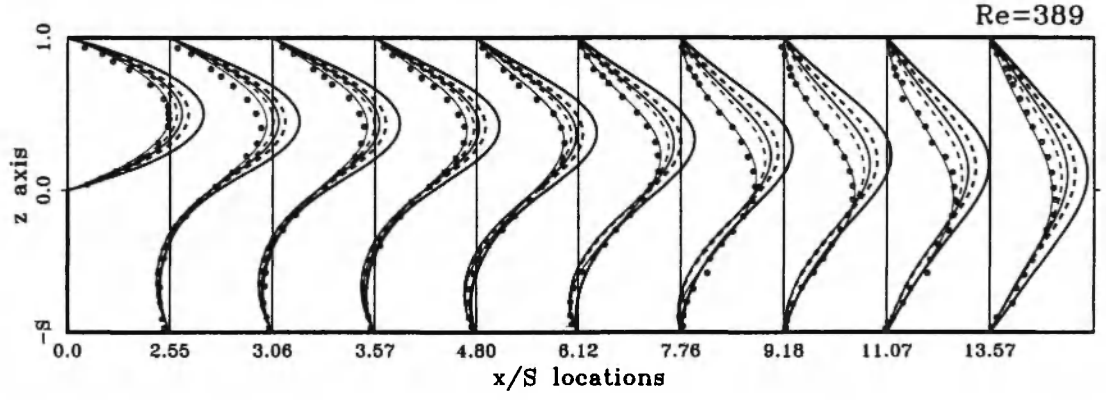

Fig. 4: Comparison study of streamwise-velocity profiles with those of Armaly *et al.* at the symmetry plane for the case conditions of Re = 389 and B = 2, 4, 6, 10, and ∞ (or 2D analysis).

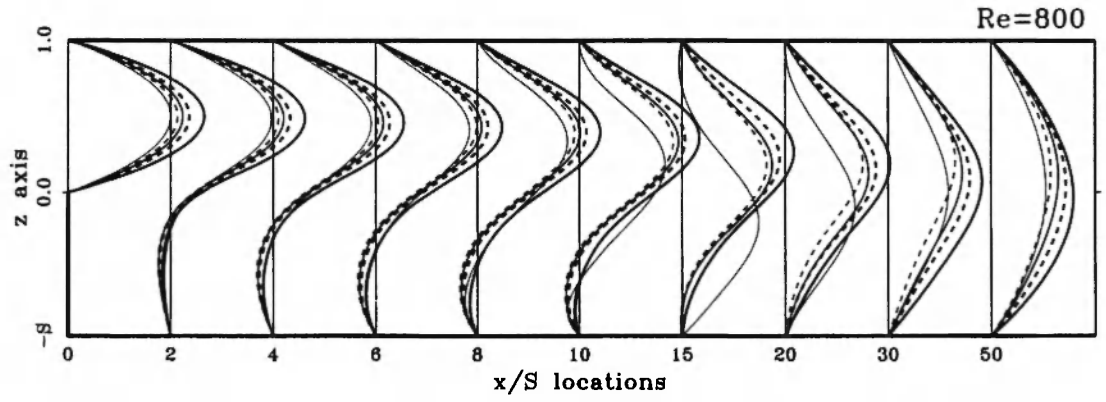

Fig. 5: Comparison study of streamwise-velocity profiles at the symmetry plane for the case conditions of Re = 800 and B = 2, 4, 6, 10, and ∞ (or 2D analysis).

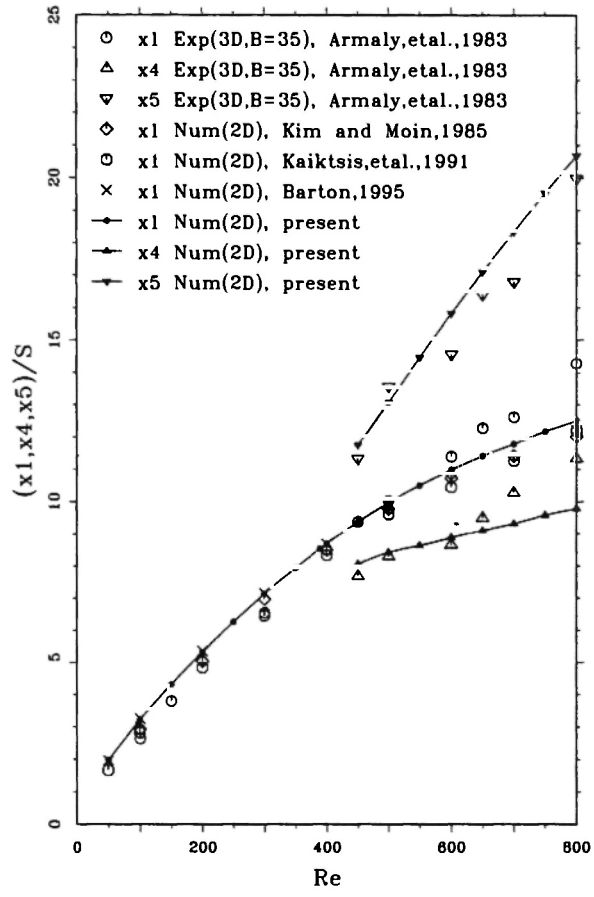

Fig. 6: A comparison study on the computed two-dimensional reattachment lengths x_1 and x_5 and the separation length x_4.

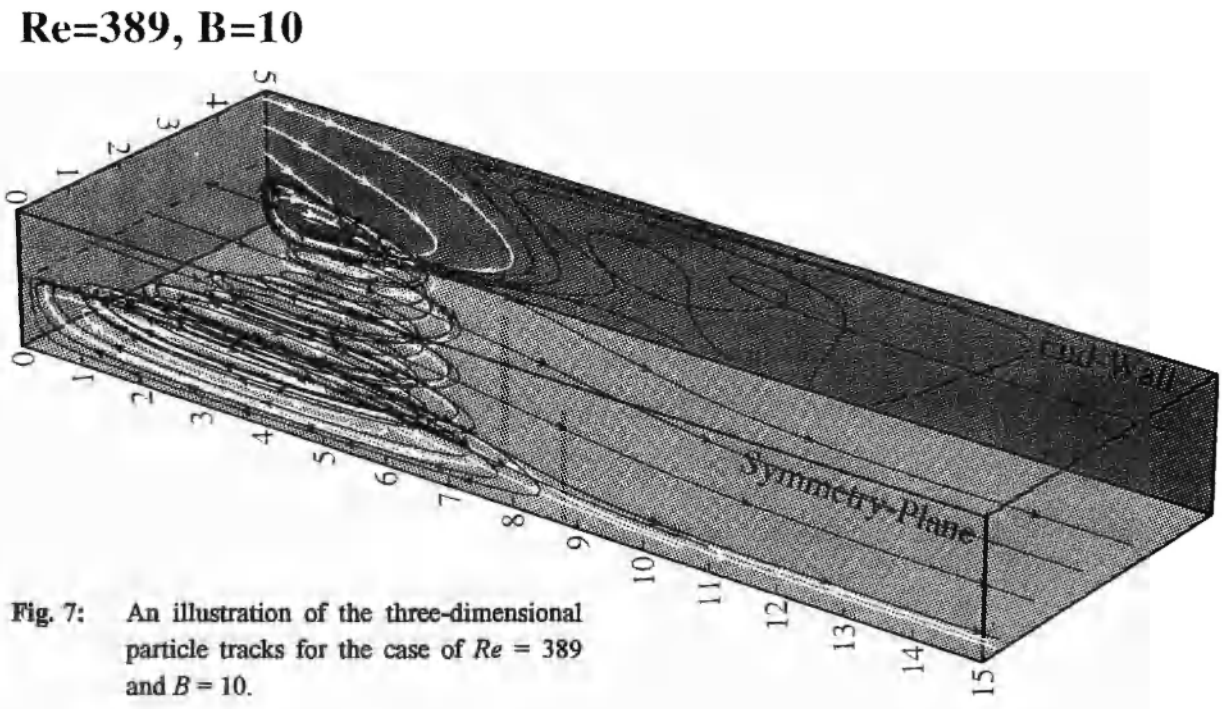

Fig. 7: An illustration of the three-dimensional particle tracks for the case of Re = 389 and B = 10.

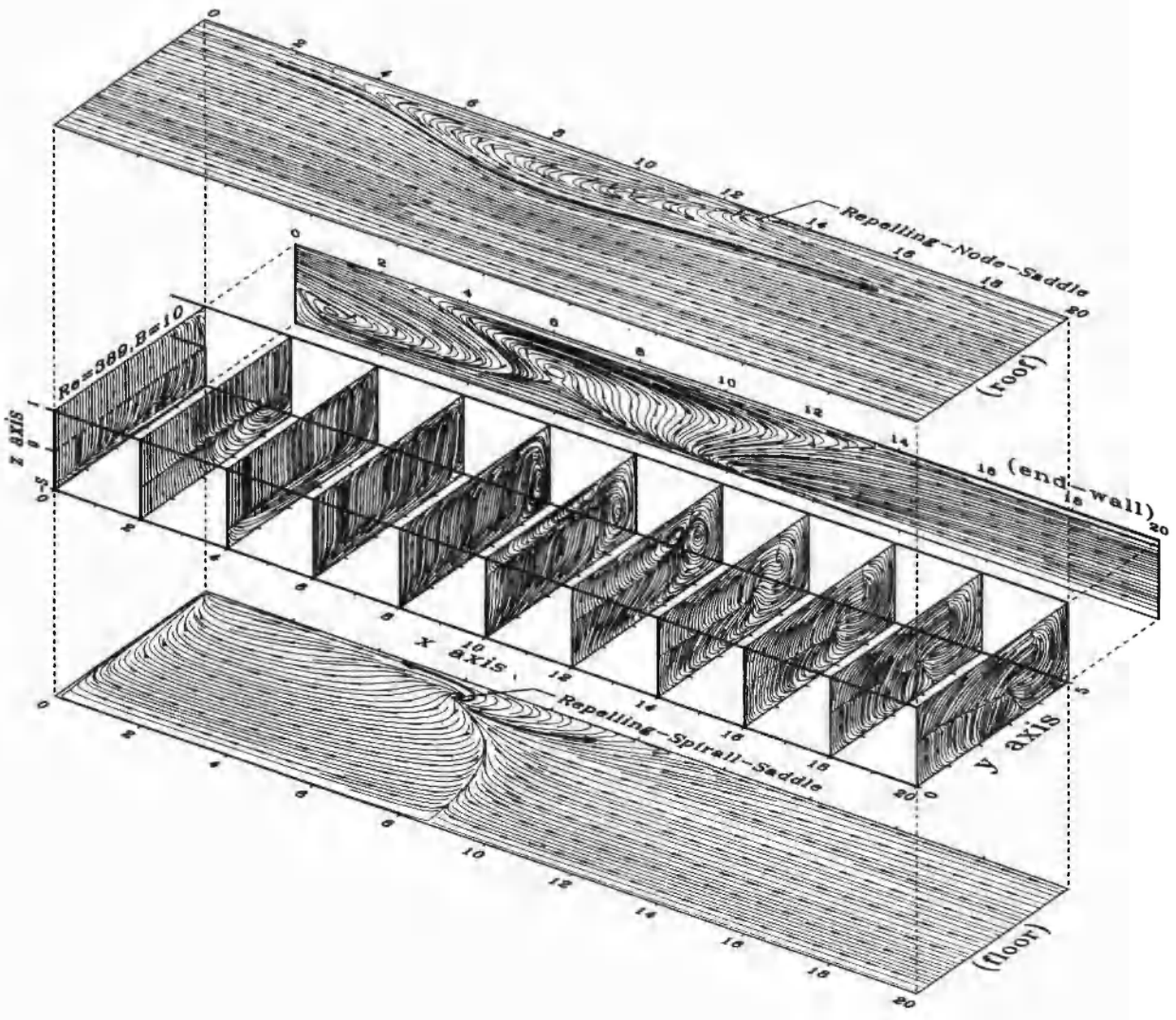

Fig. 8: The formation of the secondary flow structure at the transverse plane near the end-wall (for the case $Re = 389$ and $B = 10$).

point, classified as the saddle, is shown on a plane adjacent to the end wall. On planes in the direction normal to the end wall, we plot streamlines at different y planes, from which saddles are collected, as shown in Fig. 12. This line extends from the end wall and shows its presence within a limited range. Lines passing through saddle points are only referred to as attachment and separation lines. These two lines appear to act as barriers in the field. Along either one of these two critical lines, the direction of the flow changes sign. Both directions point towards the saddle and point away from the saddle on the other. As shown in Fig. 12, there exists a repelling focus which is situated above the saddle. This line is known as the vortical core line, which serves as a mechanism leading possibly to the global flow separation. There exists another more apparent vortical core line, which is the combination of the vortex centers of the primary eddy. Unlike the vortical core line just above the line of saddle points, this line extends over the whole span as Fig. 12 shows.

It is well accepted that a marked change, either in the shear stress distribution or in the heat transfer

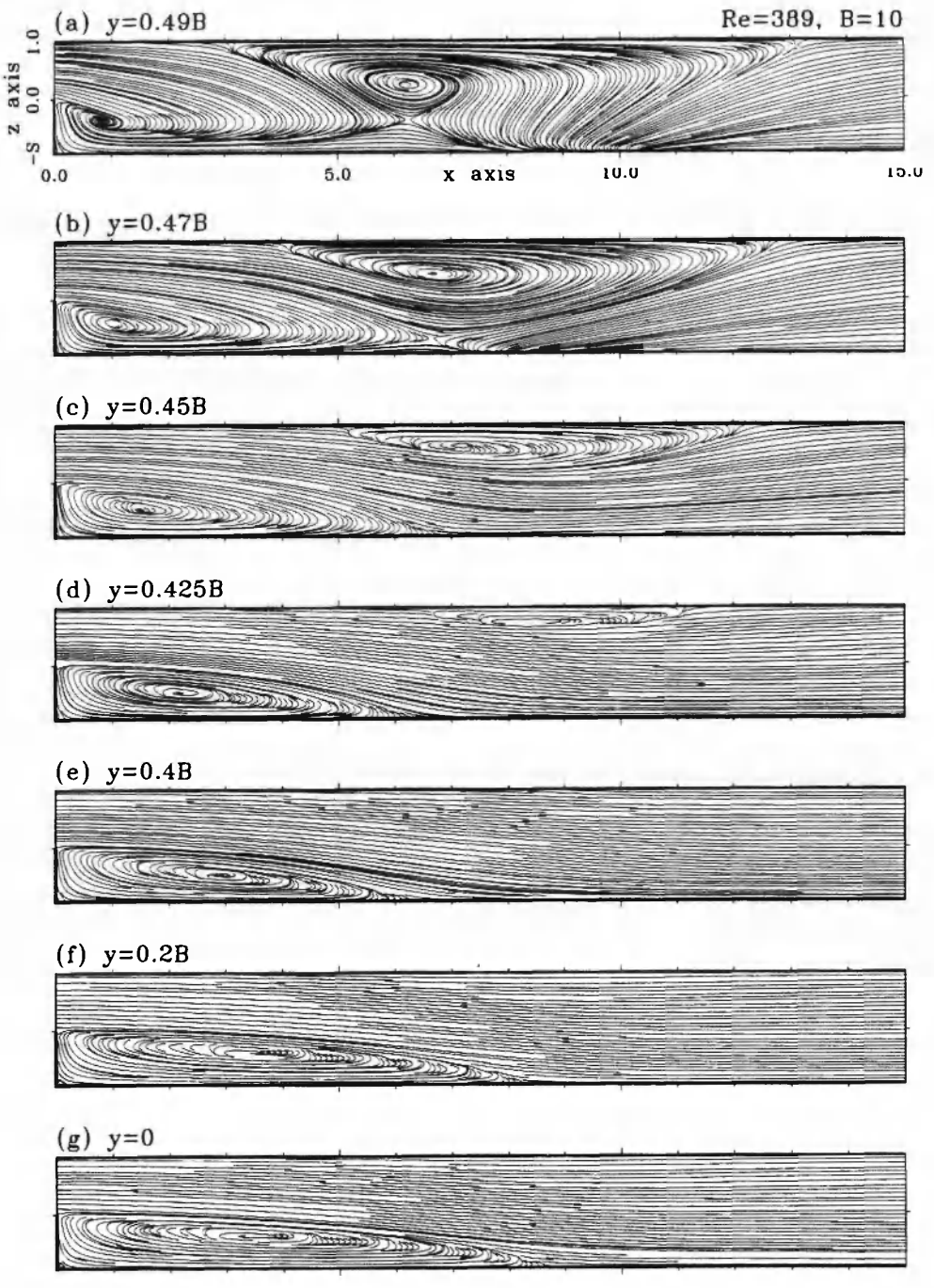

Fig. 9: The computed streamlines at x - z planes for the case of Re = 389 and B = 10.
(a) $y = 0.49B$; (d) $y = 0.425B$;
(b) $y = 0.47B$; (e) $y = 0.4B$;
(c) $y = 0.45B$; (f) $y = 0.2B$;
(g) $y = 0$.

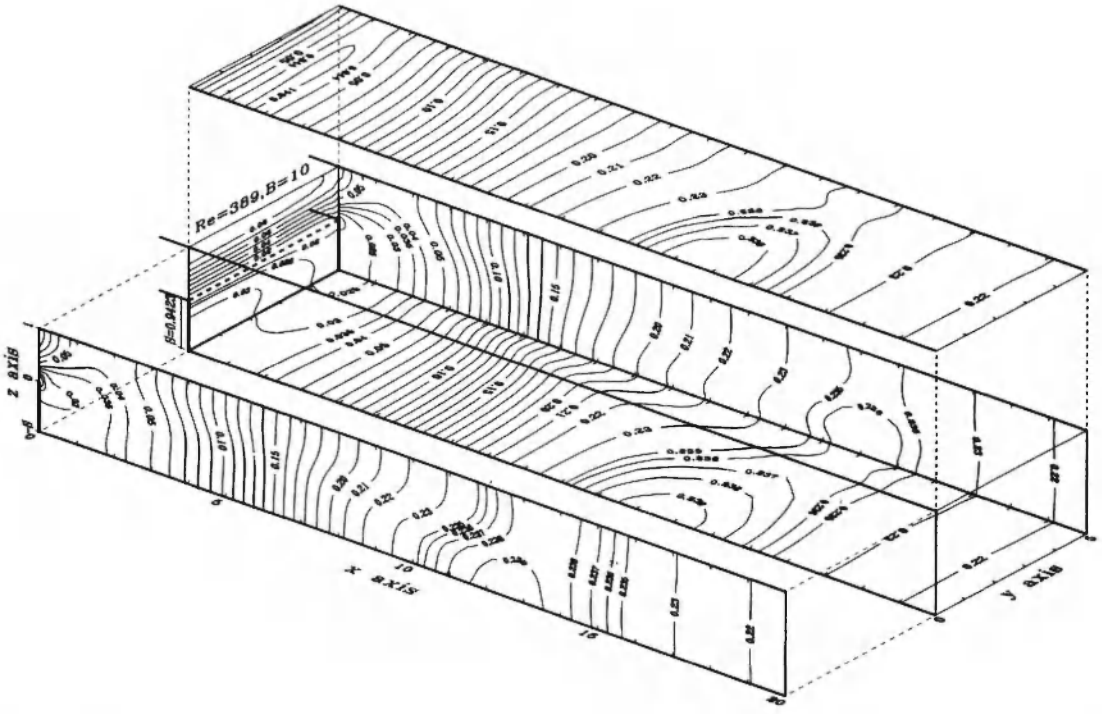

Fig. 10: Computed pressure contours on the symmetry plane, roof, floor, step-wall, and the end-wall for the case of $Re = 389$, $B = 10$.

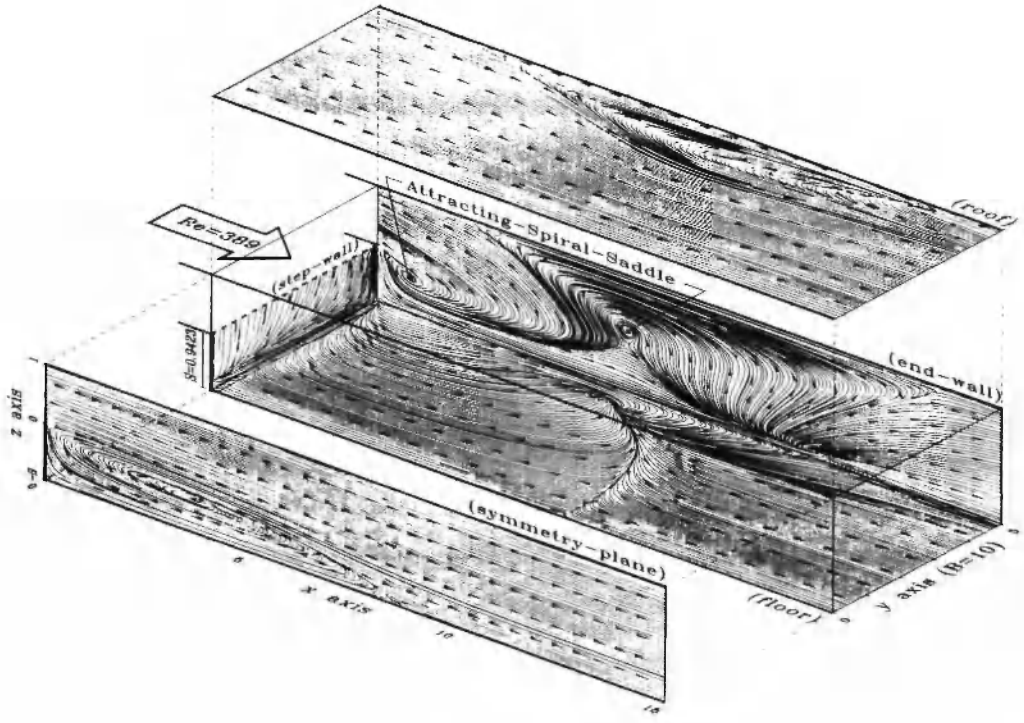

Fig. 11: A perspective view of streamlines on the symmetry plane and limiting streamlines at roof, floor, step-wall, and end-wall for the case of $Re = 389$, $B = 10$.

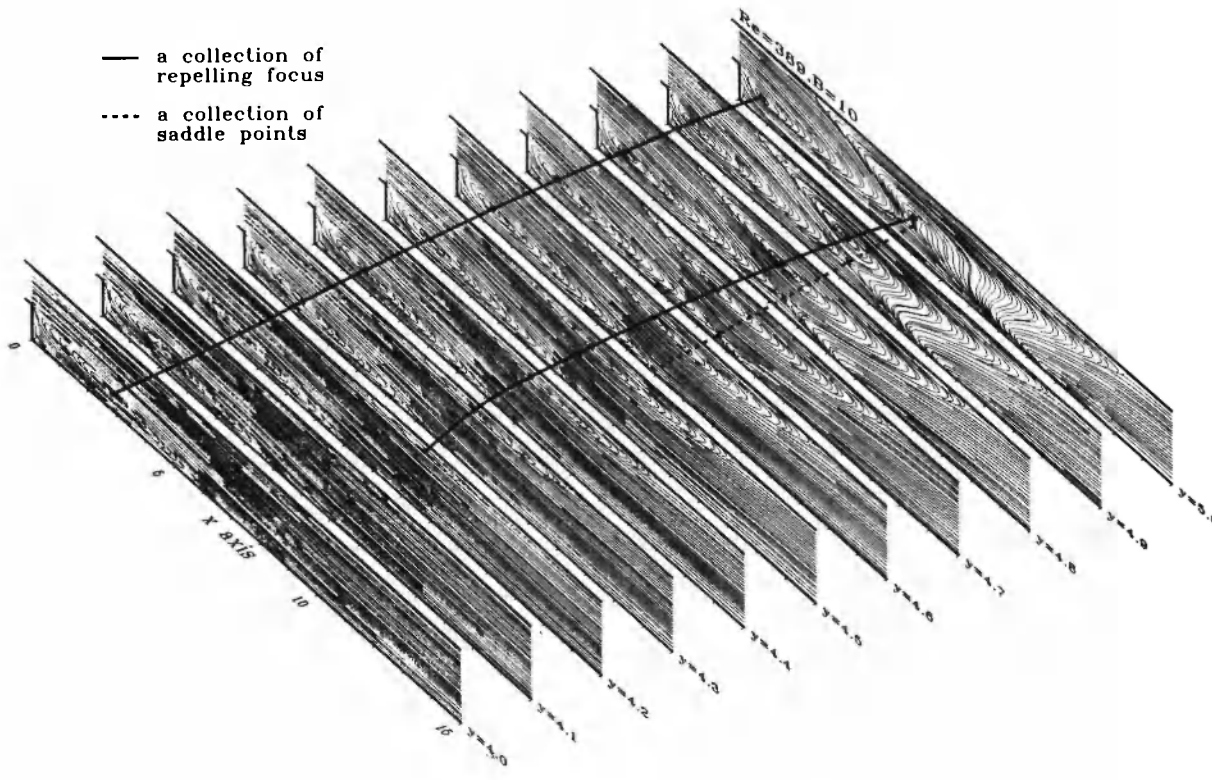

Fig. 12: A three-dimensional plot in illustration of saddle points and repelling focus for the case of $Re = 389$, $B - 10$.

rate, is a consequence of the presence of a reversal flow. Detecting the reattachment location is, thus, important for identification of the range of flow reversals. To allow for determination of three-dimensional flow separation and reattachment, we label the line of separation as the one to which streamlines converge. On the other hand, from either side of a line of attachment, streamlines tend to diverge. According to this definition, flow reattachment to the floor is seen within the half span (Fig. 13). We plot the reattachment length, x_1, as measured from the step, against spans in Fig. 14 for Reynolds numbers 100, 389, and 800. To allow for comparison with x_1 which is obtained from two-dimensional analysis, we also plot the lengths of x_1. In the presence of a primary recirculation eddy behind the step, curved streamlines in a convex form engender flow separation from the roof in the streamwise location where the separated flow reattaches to the floor. The presence of a secondary separation zone near the roof is the direct consequence of an adverse pressure gradient exerted by the sudden expansion at the step edge. The fact that the flow recovers downstream and reattaches to the upper wall is clearly from the flow separation-reattachment shown in Fig. 15. Exploiting the topological theory, we can also plot the separation length x_4 and the reattachment length x_5 as shown in Fig. 16. As with the plot of x_1, the lengths x_4 and x_5 are also measured from the step. These values are plotted against the spans for the three investigated Reynolds numbers. Beyond a small Reynolds number, say $Re = 100$, the separation-reattachment phenomenon is evident on the roof, as shown in Fig. 15. This clearly reveals the development of a three-dimensional flow, which contrasts with the two-dimensional results in that the presence of a secondary eddy is reported at Reynolds numbers as high as 450, as seen in Fig. 6.

The topological map of inferred flow patterns for

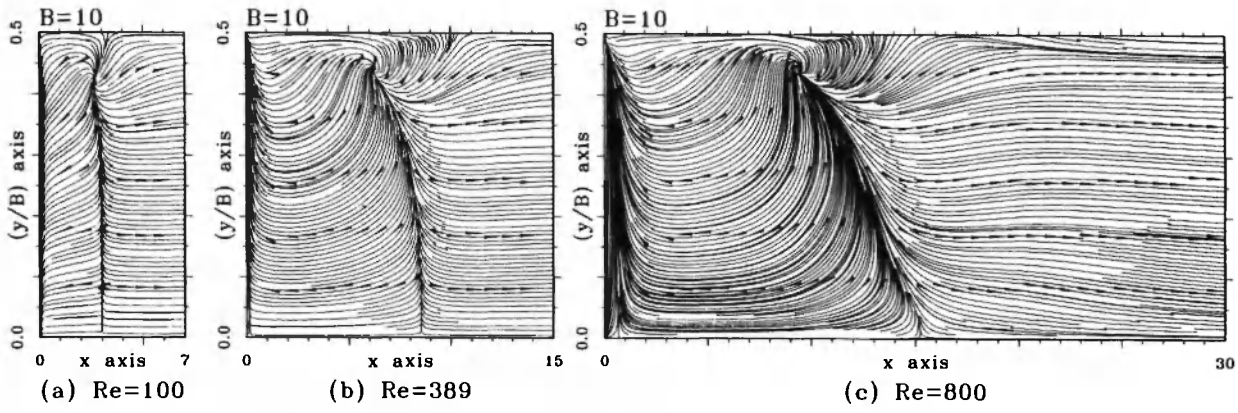

Fig. 13: The computed limiting streamlines on the floor for the case of $B = 10$.
(a) $Re = 100$;
(b) $Re = 389$;
(c) $Re = 800$.

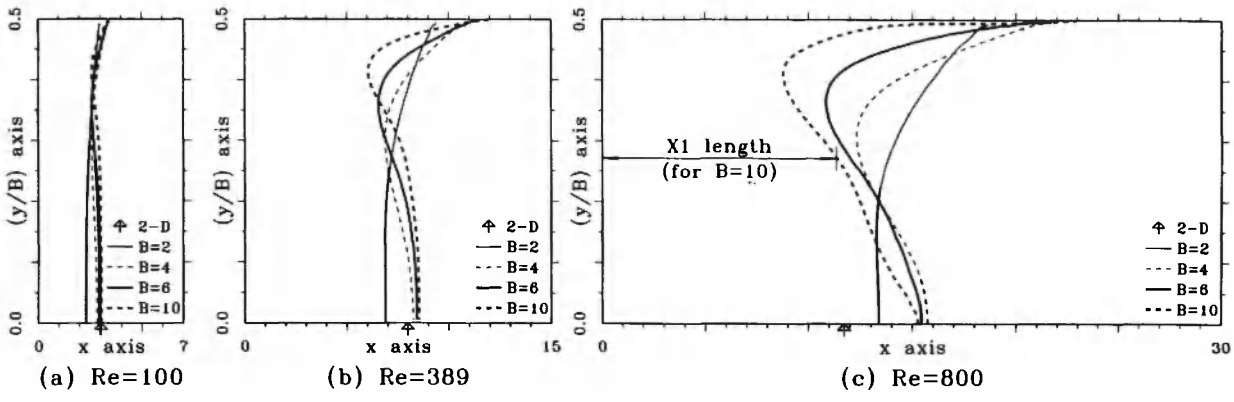

Fig. 14: The computed reattachment length x_1 against y for spans $B = 2, 4, 6, 10$.
(a) $Re = 100$;
(b) $Re = 389$;
(c) $Re = 800$.

each case considered reveals that separation-reattachment comes into play only in flow regions near the end wall. Even for Reynolds numbers as high as 800, there is no tendency of separation-reattachment formation on the symmetry plane over the range of investigated spans. Downstream of the roof eddy, there is gradual flow development into a parabolic profile. In recirculating flows, flow reversal or recirculation frequently involves the co-existence of several singular points. For example, one can clearly singular see points in the close-up plots. As Fig. 17 indicates, singular points of different classes are visible.

5. Concluding Remarks

This paper has presented some three-dimensional basic flow structures pertinent to the backward-facing step problem. The numerical method

employed here has been verified and further assessed by conducting a rate of convergence test. In an attempt to better understand the inherent three-dimensional kinematically possible flow, we have adopted a method which accommodates a sound theoretical foundation. By appealing to the topological theory in examining continuous vector three-dimensional fields, we can identify not only saddle points, but also vortical core lines inside the channel. These findings help to show that the flow unsteadiness is due naturally to the formation of a global line of separation. Also, the separation line on the bottom wall and the separation proceeding continuously with the attachment line on the upper wall of the channel can be precisely determined. To extend our understanding of the flow reversal inside a channel having a backward-facing step, we have carried out a parametric study based on Reynolds numbers not greater than 800, and spans with maximum values as high as 10. Two conclusions can be drawn from this parametric study. For the Reynolds numbers investigated, the flow tends to

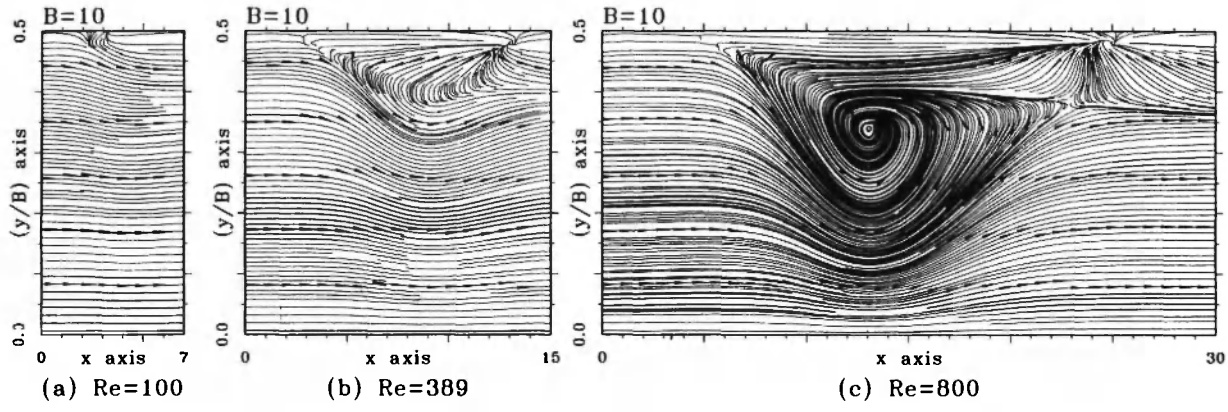

Fig. 15: The computed limiting streamlines on the roof for the case of $B = 10$.
(a) $Re = 100$;
(b) $Re = 389$;
(c) $Re = 800$.

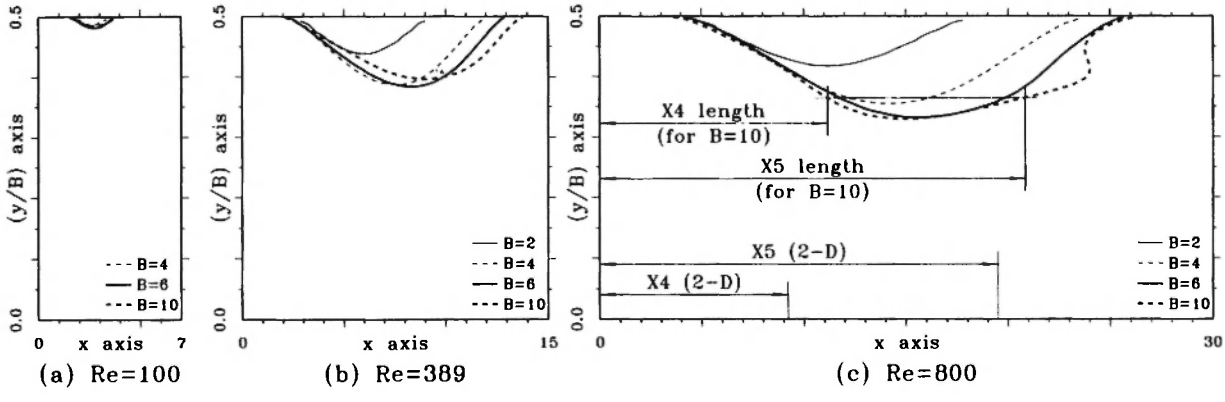

Fig. 16: The computed separation length x_4 and reattachment length x_5 against y for spans $B = 2, 4, 6, 10$.
(a) $Re = 100$;
(b) $Re = 389$;
(c) $Re = 800$.

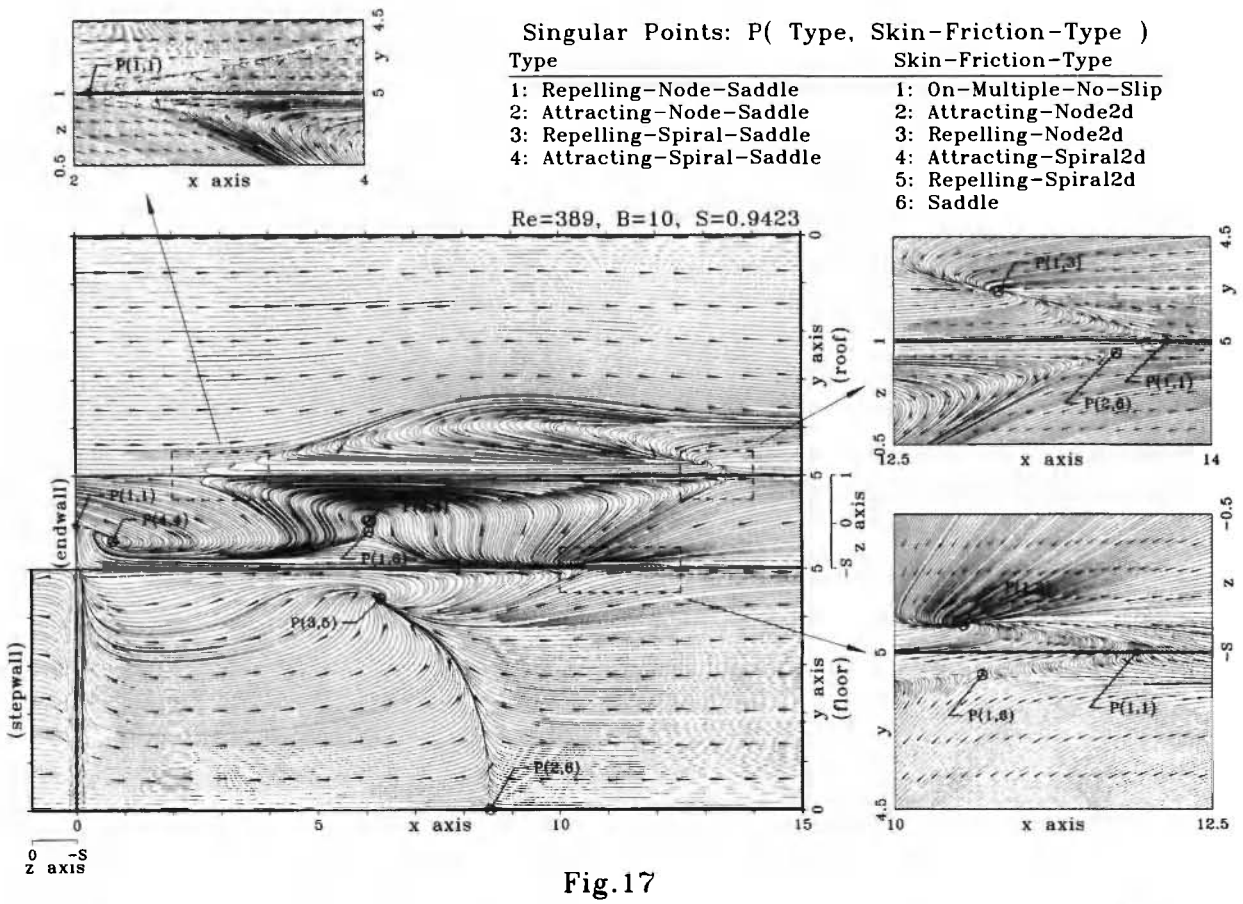

Fig.17

Fig. 17: Illustration of the computed singular points from the limiting streamlines for the case of Re = 389 and B = 10.

show a two-dimensional flow feature with an increase of the span of the channel. Secondly, a three-dimensional flow structure is manifested by a spanwise spiraling flow behind the step. It is notable that particles spiral toward the symmetry plane with increasing radius. Particles of this kind are located only near the two end walls.

Acknowledgments

This work was supported by the National Science Council under Grant NCHC85-04-004.

References

1. K. Morgan, J. Periaux and F. Thomasset (Eds.), *Analysis of Laminar Flow over a Backward Facing Step,* a GAMM-Workshop, Friedr View & Sohn, Germany, 1984.
2. L. Kaiktsis, G.E.M. Karniadakis and S.A. Orszag. Onset of three-dimensionality, equilibria, and early transition in flow over a backward-facing step, *J. Fluid Mech.,* **231**, 501 (1991).
3. B.F. Armaly, F. Durst, J.C.F. Pereira and B. Schonung. Experimental and theoretical investigation of backward-facing step, *J. Fluid Mech.,* 127, 473 (1983).
4. R.J. Goldstein, V.L. Eriksen, R.M. Olson and E.R.G. Eckert. Laminar separation reattachment, and transition of flow over a downward-facing step, *Trans. ASME D: J. Basic Engrg.,* **92**, 732 (1970).
5. Chiang Shih and Chih-Ming Ho. Three-

dimensional recirculation flow in a backward facing step, *ASME J. Fluids Engineering*, 116, 228 (1994).

6. Jung Yue Yoo and Se Jin Baik. Redeveloping turbulent boundary layer in the backward-facing step flow, *ASME J. Fluids Engineering*, 114, 522 (1992).
7. M.V. Ötiigen. Expansion ratio effects on the separated shear layer and reattachment downstream of a backward-facing step, *Experiments in Fluids*, **10**, 273 (1991).
8. G. Papadvpoulos, M.V. Ötiigen. Separating and reattaching flow structure in a suddenly expanding rectangular duct, *J. Fluids Engineering*, 117, 17 (1995).
9. J. Kim, S.J. Kline and J.P. Johnston. Investigation of a reattaching turbulent shear layer: flow over a backward-facing step, *ASME J. Fluids Engineering*, **102**, 302 (1980).
10. J. Kim and P. Moin. Applications of a fractional-step method to incompressible Navier-Stokes equations, *J. Comput. Phys.*, **59**, 308 (1985).
11. H.C. Ku, R.S. Hirsh, T.D. Taylor and A.P. Rosenburg. A pseudo spectral matrix element method for solution of three-dimensional incompressible flows and its parallel implementation, *J. Comput. Phys.*, **83**, 260 (1989).
12. D. Kwak and J.L.C. Chang. A three dimensional incompressible Navier-Stokes flow solver. Part 1 – 2NS3D code, *CFD Workshop, University of Tennessee Space Institute*, Tullahoma, TN, 1985.
13. P.T. Williams and A.J. Baker. Incompressible computational fluid dynamics and the continuity constraint method for the three-dimensional Navier-Stokes equations, *Numerical Heat Transfer, Part B*, 29, 137 (1996).
14. T. Ikohagi, B.R. Shin and H. Daiguji. Application of an implicit time-marching scheme to a three-dimensional incompressible flow problem in curvilinear coordinate systems, *Comput. Fluids*, **21** (2), 163 (1992).
15. P.T. Williams and A.J. Baker. Numerical simulations of laminar flow over a 3D backward-facing step, submitted to *Int. J. Numer. Meth. Fluids* (1995).
16. T.P. Chiang and Tony W.H. Sheu. Vortical flow over a 3D backward-facing step, *Numerical Heat Transfer, Part A: Application* (in press).
17. T.P. Chiang, Tony W.H. Sheu and S.F. Tsai. Topological flow structure in channel flows with backward-facing step, *Computers & Fluids* (in press).
18. Tony W.H. Sheu and T.P. Chiang. Spanwise motion in a three-dimensional rectangular channel having a backward-facing step, *Proceedings of the Third Int. Symp. on Experimental and Computational Aerothermodynamics of Internal Flows, September 1-6, 1996, Beijing, China*, Shen Yu Ital (Ed.), pp. 475-481.
19. O.A. Ladyzhenskaya. *Mathematical Problem in the Dynamics of a Viscous Incompressible Flow*, Gordon & Breach, New York, 1963.
20. F.H. Harlow and J.E. Welch. Numerical calculation of time-dependent viscous incompressible flow of fluid with free surface, *Phys. Fluids*, **8**, 2182 (1965).
21. S.V. Patankar. *Numerical Heat Transfer and Fluid Flow*, Hemisphere, 1980.
22. B.P. Leonard. A stable and accurate convective modeling procedure based on quadratic upstream interpolation, *Comput. Methods Appl. Mech. Engrg.*, 19, 59 (1979).
23. Y. Levy, D. Degani and A. Seginer. Graphical visualization of vortical flows by means of helicity, *AIAA J.*, **28** (8), 1347 (1990).
24. R. Legendre. Séparation de courant l'écoulement laminaire tridimensionnel, *Rech. Aéro*, **54**, 3 (1956).
25. M. Lighthill. Attachment and separation in three-dimensional flow, in: *Laminar Boundary Layers*, Vol. II, 2.6: 72-82. L. Rosenhead, Ed., Oxford University Press, 1963.
26. L.A. Yates and G.T. Chapman. Streamlines, vorticity lines and vortices around three-dimensional bodies, *AIAA J.*, **30** (7), 1819 (1992).

27. H. Poincare. Sur les courbes defines par une equation differentiette, *J. Math.*, **1**, 167 (1875).
28. G. Bancroft, F. Merritt, T. Plessel, P. Kelaita, R. McCabe and A. Globus. FAST: A multi-processing environment for visualization of CFD, *Proc. Visualization '90,. IEEE Computer Society*, San Francisco, 1990.
29. C.R. Ethier and D.A. Steinman. Exact fully 3D Navier-Stokes solutions for benchmarking, *Int. J. Numer. Meths. in Fluids*, **19**, 369 (1994).